Prediction of solvent-induced morphological changes of polyelectrolyte diblock copolymer micelles

ARTICLE *in* SOFT MATTER · AUGUST 2015

Impact Factor: 4.03 · DOI: 10.1039/c5sm01742d · Source: PubMed

7 AUTHORS, INCLUDING:

Lei Tang

Duke University

8 PUBLICATIONS **150** CITATIONS

SEE PROFILE

Ashutosh Chilkoti

Duke University

292 PUBLICATIONS **15,007** CITATIONS

SEE PROFILE

Stefan Zauscher

Duke University

112 PUBLICATIONS **4,230** CITATIONS

SEE PROFILE

Yaroslava G Yingling

North Carolina State University

77 PUBLICATIONS **1,112** CITATIONS

SEE PROFILE

Soft Matter

PAPER

View Article Online
View Journal

Cite this: DOI: 10.1039/c5sm01742d

Prediction of solvent-induced morphological changes of polyelectrolyte diblock copolymer micelles†

Nan K. Li,[a] William H. Fuss,[a] Lei Tang,[b] Renpeng Gu,[b] Ashutosh Chilkoti,[c] Stefan Zauscher[b] and Yaroslava G. Yingling*[a]

Received 14th July 2015,
Accepted 18th August 2015

DOI: 10.1039/c5sm01742d

www.rsc.org/softmatter

Self-assembly processes of polyelectrolyte block copolymers are ubiquitous in industrial and biological processes; understanding their physical properties can also provide insights into the design of polyelectrolyte materials with novel and tailored properties. Here, we report systematic analysis on how the ionic strength of the solvent and the length of the polyelectrolyte block affect the self-assembly and morphology of the polyelectrolyte block copolymer materials by constructing a salt-dependent morphological phase diagram using an implicit solvent ionic strength (ISIS) method for dissipative particle dynamics (DPD) simulations. This diagram permits the determination of the conditions for the morphological transition into a specific shape, namely vesicles or lamellar aggregates, wormlike/cylindrical micelles, and spherical micelles. The scaling behavior for the size of spherical micelles is predicted, in terms of radius of gyration ($R_{g,m}$) and thickness of corona (H_{corona}), as a function of solvent ionic strength (c_s) and polyelectrolyte length (N_A), which are $R_{g,m} \sim c_s^{-0.06} N_A^{0.54}$ and $H_{corona} \sim c_s^{-0.11} N_A^{0.75}$. The simulation results were corroborated through AFM and static light scattering measurements on the example of the self-assembly of monodisperse, single-stranded DNA *block*-copolynucleotides (polyT50-*b*-F-dUTP). Overall, we were able to predict the salt-responsive morphology of polyelectrolyte materials in aqueous solution and show that a spherical–cylindrical–lamellar change in morphology can be obtained through an increase in solvent ionic strength or a decrease of polyelectrolyte length.

Introduction

Polyelectrolyte diblock copolymers (PDCs), which combine the properties of polyelectrolytes (*i.e.*, sensitive to changes in solvent ionic strength and pH) with those of surfactants, can self-assemble in an aqueous environment into a variety of responsive morphologies, including spherical micelles, star-like/hairy and crew-cut, cylindrical micelles, vesicles, lamellar mesophases, and micellar aggregates.[1–3] Such assemblies are promising candidates as carriers for drug and gene delivery, where the morphology and the size of the assemblies determine their transport properties and delivery capabilities.[4] For example, it was suggested that cylindrical delivery vehicles display a longer circulation time in the body than spherical carriers, due to reduced interactions with the blood vessel walls.[5] Aside from biomedical applications, preparation of micelles with various morphologies is also important in the fabrication of soft lithography templates.[6,7] Ability to predict and control the responsive morphology of PDCs is needed for the development of new materials systems with a broad range of biological and technological applications.[8,9]

Many experimental studies have been focused on the investigation of the structure and properties of micellar solutions of various polyelectrolyte block copolymers.[10–15] It was determined that increasing the solvent ionic strength induces the shrinkage of corona chains, increases the micellar aggregation number, and alters the micellar morphology.[3,16,17] However, the mechanism controlling self-assembly, aggregation and overall morphology of polyelectrolyte block copolymers is complex and is largely driven by the characteristically intricate equilibrium of non-covalent interactions, including electrostatic, steric, hydrophobic, van der Waals interactions, and hydrogen bonding.[18] With the rapidly growing ability to synthesize PDCs with specific size and dispersity, it is important to develop a comprehensive method

[a] Department of Materials Science and Engineering, North Carolina State University, 911 Partners Way, Raleigh, NC 27695, USA. E-mail: yara_yingling@ncsu.edu
[b] Department of Mechanical Engineering and Materials Science, Duke University, 144 Hudson Hall, Durham, NC 27708, USA
[c] Department of Biomedical Engineering, Duke University, 136 Hudson Hall, Durham, NC 27708, USA

† Electronic supplementary information (ESI) available: Additional experimental and simulations details, such as complete morphological diagrams, extra analysis on the size of micelles, effect of concentration, AFM images and measurements are available. See DOI: 10.1039/c5sm01742d

that is able to predict the solvent-dependent properties, morphologies, and assembly kinetics of these molecular assemblies.

Mean-field theories and scaling theories can be used to describe the properties of PDC micelles.[19–22] One of the most notable theories is the one developed by Borisov and Zhulina which is based on the mean-field theory.[18,21] In this theory, the free energy of the micelles is described in terms of the degree of polymerization of the polyelectrolyte and hydrophobic blocks, and several external parameters that control the interaction strength, such as the second virial coefficient, which represents non-electrostatic excluded-volume interactions, and the Coulomb interactions between the charged monomers. Although, morphological transitions were predicted through the free energy expressions for spherical, cylindrical, or lamellar micelles, according to their respective packing geometries,[18,21] theoretical analysis of the self-assembly and morphology of PDCs is challenging compared to that of neutral systems and more developments in this area are needed.[23]

Computational techniques can be used to elucidate the processes and mechanisms of the self-assembly of amphiphilic components in solution and are a valuable complement to experimental and theoretical approaches.[24–27] However, the use of computational and modeling techniques for self-assembly of polyelectrolyte block copolymers in aqueous solution has not been extensively explored, despite the significant interest in tailoring polyelectrolytes systems for various applications. All-atom simulations of the self-assembly of many polyelectrolyte chains are computationally expensive, because the size of the system, as well as the equilibration and residence times of counterions, can be prohibitively large.[28–30] Therefore, to achieve a balance between reasonable physical description and computational feasibility, a commonly used strategy to simulate these processes is to use coarse-grained modeling techniques, such as coarse-grained molecular dynamics (MD) or Dissipative particle dynamics (DPD).[31] However, modeling of complex polyelectrolyte systems in aqueous solution is challenging and computationally intensive even for coarse-grained models due to the implementation of long range electrostatic interactions.[32] Only a few of such simulation studies have been reported where the system size was relatively small and the interactions between a scarce number of polyelectrolyte molecules were investigated.[33–37] In terms of predicting and observing morphological changes of PDCs as a function of ionic strength and pH, the most notable study is the recent work by Pantano *et al.* where coarse-grained MD simulations were used to reproduce different morphologies of short, charged diblock copolymers due to changes in pH and the presence of Ca^{2+}.[38] To the best of our knowledge there are no comprehensive, large-scale comprehensive computational studies on the prediction of self-assembly and morphology of PDC micelles with polyelectrolyte corona.

To overcome the current computational limitations, we have recently developed a new implicit solvent ionic strength (ISIS) methodology for the DPD method which combines the explicit solvent with the implicit ionic strength representation and permits large-scale simulation of self-assembling polyelectrolytes and their response to the changes in ionic strength, especially at the salt-dominated regime.[39] Briefly, in our model we parameterize the repulsive non-bonded parameter (a_{pp}), between and within the polyelectrolyte chains in analogy with a second virial coefficient formalism for a good solvent based on mean-field theory for polyelectrolyte systems. Our coarse-grained modeling methodology is designed for studies of large-scale systems that involve the ionic strength-dependent behavior of strong polyelectrolytes (*i.e.* DNA, RNA, poly(styrenesulfonate), *etc.*), which is currently unreachable by other computational methods, and enables us to obtain important descriptors of micelle morphology and structure, *i.e.*, the aggregation number, the corona and core sizes, and micelle anisotropy, as a function of polyelectrolyte block length and solvent ionic strength.

In this paper, we use our ISIS DPD model to predict the ionic strength-dependent morphology of highly asymmetric, PDCs in aqueous solution. Specifically, we explore the role of polyelectrolyte block length and solvent ionic strength on the morphological properties of the assemblies. The diblocks have a short hydrophobic block with a fixed degree of polymerization, $N_B = 4$, and a variable length of the hydrophilic block with a degree of polymerization, N_A, ranging from 4 to 90 (Fig. 1a). To validate our predictions, we examine the self-assembly of asymmetric, 54-mer single stranded DNA (ssDNA) amphiphiles using static light scattering (SLS) and AFM imaging, and compare the results to the simulation predictions. These polyelectrolyte amphiphiles were synthesized by appending on average about four hydrophobic nucleotides (*i.e.*, Fluorescein-dUTP) to the 3′ termini of hydrophilic polynucleotides ($polyT_{50}$) *via* an enzymatic polymerization reaction.[24] In aqueous solution, the hydrophobic F-dUTP segments aggregate and form the micellar core. Overall, we demonstrated the ability to predict the morphology of PDCs in aqueous solution and their response to a change in solvent ionic strength.

Experimental section

Simulation method

All simulations were performed using Dissipative particle dynamics (DPD) *via* LAMMPS.[40,41] DPD is a coarse-grained simulation technique in which one DPD bead represents a group of atoms or a volume of fluid that is large on the atomistic scale but still macroscopically small.[42,43] All beads move according to Newton's equations of motion, $m_i\frac{dv_i}{dt} = \sum_{j\neq i} f_{ij}$, where m_i, r_i and v_i are the mass, position, and velocity of bead i. The DPD potential consists of three pairwise forces between DPD beads, *i.e.*, the conservative, the dissipative, and the random force. The force acting on a bead is given by $f_{ij} = F_{ij}^C + F_{ij}^D + F_{ij}^R$. All forces vanish beyond a certain cutoff radius, r_c. The conservative force F_{ij}^C determines the thermodynamics of the DPD system, and is defined by a purely repulsive (parabolic) soft-core potential, given by $F_{ij}^C = a_{ij}(1 - r_{ij}/r_c)\bar{r}_{ij}$, $r_{ij} < r_c$. a_{ij} is the maximum repulsion between beads i and j; $\mathbf{r_{ij}} = r_i - r_j$, $r_{ij} = |\mathbf{r_{ij}}|$, $v_{ij} = v_i - v_j$, and $\bar{r}_{ij} = \mathbf{r_{ij}}/r_{ij}$ is the unit vector directed along j to i. The dissipative force is $F_{ij}^D = -\gamma w^D(r_{ij})(\bar{r}_{ij}\cdot v_{ij})\bar{r}_{ij}$ and the random force is $F_{ij}^R = \sigma_D w^R(r_{ij})\theta_{ij}\Delta t^{-\frac{1}{2}}\bar{r}_{ij}$,

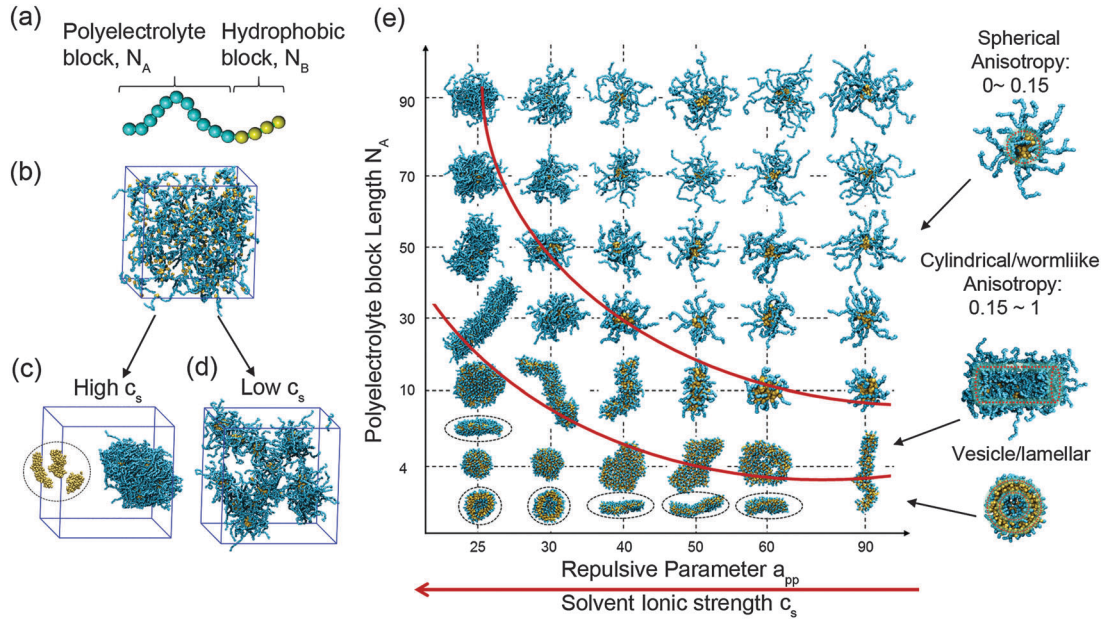

Fig. 1 (a) Representation of a PDC chain. Simulation snapshots of initial (b) and final configurations at (c) a_{pp} = 25 and (d) a_{pp} = 40 with N_A = 50 and N_B = 4. The cyan and yellow beads represent the hydrophilic and hydrophobic block, respectively. (e) Phase diagrams of typical aggregates of PDCs obtained by DPD simulations. The section views for vesicles and side views for lamellar shapes are marked by the dashed circles and ellipsoids. The phase diagrams of final snapshots of PDCs in aqueous solutions are displayed in Fig. S1 (ESI†).

where coefficients γ and σ_D characterize the strengths of the dissipative and random forces, and $\gamma = \frac{\sigma_D{}^2}{2k_BT} = 4.5$. $\theta_{ij}(t)$ is a zero-mean symmetric random variable. We use $w^D(r_{ij}) = [w^R(r_{ij})]^2 = (1 - r_{ij}/r_c)^2$ to ensure momentum conservation. Also the properties of the system are expressed using dimensionless quantities in units of the cutoff r_c, the energy scale k_BT and the bead mass m_0. As a consequence, the unit of time, τ, is $\tau = \sqrt{r_c{}^2 m_0/k_BT}$. Time evolution of the system was calculated by the Verlet algorithm with a time step $\Delta t = 0.05\tau$, where τ is the DPD unit of time. The total bead number density in the simulation system is $\rho = 3$.

One of the major advantages of DPD is the intuitiveness and ease with which simple models for various complex fluids can be constructed by modifications of the conservative interactions (repulsive parameter a_{ij}) between DPD beads, although there is certain limitation for DPD fluid to exhibit a rigid thermodynamic behavior of the system.[44,45] However, it was demonstrated that the coarse-grained mesoscopic model can correctly reproduce the properties and phase behavior of a system beyond certain length and time scales.[46–48]

The incorporation of electrostatic interactions into DPD was originally proposed by Groot,[33] whose model is based upon the particle–particle particle–mesh (PPPM) method with a charge distribution function adapted for the use of soft potential. The second approach for the implementations of electrostatics was developed by Gonzáles-Melchor and co-workers,[49] using the Ewald technique[50] with a charge distribution on DPD beads. DPD is extremely efficient in comparison with molecular dynamics (MD), but the implementation of long range electrostatic interactions considerably increases the computational cost and complexity of DPD. We thus developed a new methodology for DPD for the modeling and simulation of polyelectrolyte systems with implicit representation of ionic strength in the explicit solvent, which can efficiently capture salt-dependent conformational features of large-scale polyelectrolyte systems in aqueous solutions. Here, the ISIS DPD model is applied to study the effect of solvent ionic strength on the self-assembly of polyelectrolyte block copolymers where the repulsive parameter between polyelectrolytes in DPD is approximated with a second virial coefficient formalism in good solvent.[39] The DPD conservative force produces an equation of state (EOS) that can be expressed by $p = \rho k_BT + \alpha a\rho^2$ ($\alpha = 0.101 \pm 0.001$), as the virial expansion with pressure p, density ρ, and repulsive parameter $a = a_{ij}$, which works very well for $\rho \geq 3$ and $a \geq 15$.[43] Thus, a good approximation for the soft potential parameter a_{ij} that holds for sufficiently high density could be $a_{ij} \sim \nu$, where ν is the second virial coefficient. If $\rho = 3$, the repulsion parameter between beads of the same type is $a_{ii} = 25$ based on the Groot and Warren[43] scheme. In the case of polyelectrolytes in a salt-dominated environment, *i.e.*, where the bulk concentration of added salt exceeds the concentration of counterions, the short-range repulsion between charged monomers is governed by the screened Coulomb interactions (by salt) and complemented by the non-electrostatic (excluded volume) interactions. Based on the mean-field approximation, the effective second virial coefficient calculated per monomer is then equal to:[18,21]

$$\nu = \nu_A + \alpha^2/c_s \quad (1)$$

where ν_A is the bare non-electrostatic contribution to the second virial coefficient, α is the degree of ionization, and c_s is the solvent ionic strength.

Analogous to the second virial coefficient, ν, in ISIS DPD model, we represent the repulsive parameters between polyelectrolyte beads as:

$$a_{pp} = a_{ii} + a_{elec} \quad (2)$$

$$a_{elec} \sim c_s^{-1} \quad (3)$$

where $a_{ii} = 25$ (at $\rho = 3$). Only when the solvent ionic strength is extremely high, $a_{elec} \rightarrow 0$, the behavior of polyelectrolytes is reduced to that of neutral polymers with the same solvation properties.

The ISIS DPD model was previously[39] benchmarked on the dynamics of a single, long polyelectrolyte chain (300-mer) and the self-assembly of polyelectrolyte diblock copolymers (34-mer) in aqueous solutions with variable ionic strength. The main advantages of our model are its computational speed and simplicity of implementation which enables the intensive study of the self-assembly behaviors of polyelectrolyte block copolymers at high solvent ionic strength. The main limitation of our ISIS model is that the radial gradients in the polyelectrolyte density and mobile ion distribution are neglected due to the mean-field and local electroneutrality approximations made in the derivation of this methodology. However, this effect is negligible when the polyelectrolyte chain is in salt-dominated regime, which is the case of our study. This model is suitable for studies of processes and properties of various systems containing strong polyelectrolytes (DNA, RNA, poly(styrenesulfonate), *etc.*) in salt-dominated condition.

As shown in Fig. 1a, each polyelectrolyte diblock copolymer chain is composed of a hydrophobic block with a degree of polymerization $N_B = 4$, and a hydrophilic polyelectrolyte block with the variable degree of polymerization N_A, ranging from 4 to 90. In our system, the amphiphilic chains are represented as a bead-spring type particle model, where adjacent beads in the chains are connected *via* an extra harmonic spring: $F_{ij}^S = Cr_{ij}$, where the spring constant C is set to 4.0 for bonds linking hydrophobic beads and 50.0 for bonds between polyelectrolyte beads to link polymer beads together in the backbone. The choice of C does not affect the qualitative behavior of the system. The repulsive parameters for the hydrophilic–hydrophobic segment interactions and water–hydrophobic interactions were set to be 90 and 100, respectively, to obtain aggregates in water. The interaction parameter between the hydrophilic polyelectrolyte segments and water molecules were set to 26.

Fig. 1b shows the initial snapshot of the system for $N_A = 50$. To illustrate the self-assembly of polyelectrolyte block copolymers, 300 chains were initially distributed randomly in a simulation box with periodic boundaries. We consider a dilute solution of block copolymers with a polymer volume fraction ranging from 0.0729 to 0.2015. The total number of beads in the system was 139 968. The phase diagram of the aqueous solution of polyelectrolyte diblock copolymers obtained by DPD simulations are displayed in Fig. S1 (ESI†). To reveal the effect of PDC concentration on the morphology of larger aggregates, we also performed simulations at a higher copolymer concentration, *i.e.*, with 600 chains. Fig. S2 (ESI†) shows the equilibrium snapshots of copolymer aggregates ($N_B = N_A = 4$).

A considerably long simulation ($>4 \times 10^6$ steps) was performed for each group to attain thermodynamic equilibrium. For example, the time evolution of aggregation number shows convergence by 3.0×10^6 steps (Fig. S3, ESI†). After equilibrium was reached, we have continually observed frequent exchanges of chains between micelles, and the outcome of the kinetic process guarantees true equilibrium. The trajectories were collected every 1000 time steps. Only the last 1.0×10^6 time steps of the trajectories from each run were considered for the statistical analysis.

In the framework of the ISIS DPD model we obtained its equilibrium characteristics as a function of the length of the hydrophilic block and ionic strength in the solution. We specifically focus here on the experimentally measurable properties of micelles: the aggregation number P (the number of chains associated into one micelle), the radius of gyration of the micelle ($R_{g,m}$) and the core ($R_{g,c}$), the thickness of the corona (H_{corona}), and the anisotropy κ^2. In some cases, multidisperse micelles were obtained in the system, especially for a spherical micelles. For example, the probability distribution of the aggregation number for $N_A = 50$ is shown in Fig. S4 (ESI†). At high solvent ionic strength $a_{pp} = 30$, aggregation number displays a wider distribution for cylindrical micelles obtained. As a_{pp} increased, the distribution of P became narrower for spherical micelles. The size parameters for multidisperse micelles were averaged for aggregates with the aggregation number $P > 5$.

After identifying all the aggregates we then calculated the radius of gyration of micelles and micellar cores as the root mean square average radial distance, or distance of every bead from the center of mass of the micelle, as shown by the following equation:

$$R_{g,m} = \sqrt{\frac{1}{N_p}\sum_{i=1}^{N_p}(r_i - r_{com})^2} \quad \text{and} \quad R_{g,c} = \sqrt{\frac{1}{N_p}\sum_{i=1}^{N_p}(r_{c,i} - r_{com})^2}.$$

The thickness of the micellar corona was determined using $H_{corona} = R_{g,m} - R_{g,c}$.

Next we constructed the gyration tensor for each micelle and determined the principal moments.[39] Using the principal moments, the calculated radius of gyration could be confirmed and the relative shape anisotropy could be calculated with the following equations:

The radius of gyration was calculated as:

$$R_g^2 = \lambda_x^2 + \lambda_y^2 + \lambda_z^2 \quad (4)$$

The relative shape anisotropy κ^2 was calculated as:

$$\kappa^2 = \frac{3}{2}\frac{\lambda_x^4 + \lambda_y^4 + \lambda_z^4}{\left(\lambda_x^2 + \lambda_y^2 + \lambda_z^2\right)^2} - \frac{1}{2} \quad (5)$$

where κ^2 is bounded between 0 and 1. $\kappa^2 = 0$ only occurs if all points are spherically symmetric, and $\kappa^2 = 1$ only occurs if all points lie on a line.

Synthesis of oligonucleotide amphiphiles T50-fluorescein

The reaction mixtures consisted of 1 μM oligonucleotide initiator, T50, fluorescein-dUTP (F-dUTP) monomer, (10 μM, for M : I ratios 10, respectively), and 800U of TdT in 1600 μl of terminal deoxynucleotidyl transferase buffer. Enzymatic polymerization

was carried out for overnight at 37 °C after which the reaction was terminated by heating at 70 °C for 10 min. The reaction products were purified by centrifugal ultrafiltration (Microcon YM-10 centrifugal filter device, Millipore), followed with dialysis in Milli-Q H_2O (Thermo Scientific Slide-A-Lyzer MINI Dialysis Devices, 2K MWCO) for two days, to remove, unreacted monomers, and salt compounds.

Static light scattering (SLS) measurements were performed using the ALV/CGS-3 goniometer system (ALV, Langen, Germany). Samples were prepared by filtering solution through an Anotop 10 Watman 200 nm filter into a 10 mm disposable borosilicate glass tube (Fischer). The SLS measurements were performed over a range of angles (30° to 150°) at 5° increments. At each angular position, intensity data from five, 3 s long, acquisition cycles were averaged. A Zimm plot was created by measuring the normalized intensity of scattered light at multiple scattering angles. After linear fitting of the equation the $R_{g,m}$ was calculated from the slope.

$$\frac{K_c}{R} = \frac{1}{M_W} + \frac{1}{3}\frac{1}{M_W} q^2 {R_{g,m}}^2 \quad (6)$$

where M_W is the weight-averaged molar mass, R is the Rayleigh ratio, q is the scattering wave vector, c is the concentration of the sample, and K is the optical constant.

AFM imaging

Samples for AFM imaging were prepared by first placing a drop of the sample solution (a mixture of polynucleotides ($\sim$0.5 μM) in a range of NaCl concentrations with 5 mM $MgCl_2$ added) onto freshly cleaved mica surfaces and incubating for 5 minutes. Then the sample was rinsed with Milli-Q H_2O and dried in a stream of dry nitrogen. Tapping Mode AFM images were acquired under ambient conditions with a MultiMode AFM (Bruker), using Tapping Mode silicon cantilevers (k_F = 40 N m^{-1}, f_{res} = 311–357 kHz, R_{tip} < 10 nm, Bruker).

Results and discussion

We systematically analyze how the solvent ionic strength (a_{pp}) of the solution, and the length of the hydrophilic polyelectrolyte block (N_A) affect the kinetics of self-assembly and the equilibrium morphology of the aggregates (Fig. 1 and Fig. S1, ESI†). The representative aggregates of PDCs obtained by DPD simulations are displayed in Fig. 1e and the morphological phase diagrams of final snapshots of PDCs in aqueous solutions are displayed in Fig. S1 (ESI†). Examination of the micellar shapes in Fig. 1e reveals that PDCs form three morphological types, *i.e.*, vesicle/lamellar aggregates, wormlike/cylindrical micelles, and spherical micelles. Increasing the repulsive parameter a_{pp} (*i.e.*, decreasing solvent ionic strength c_s) or increasing the length of the polyelectrolyte block, N_A, leads to a morphological transition from vesicle/lamellar aggregates to cylindrical and spherical micelles. The changes in micellar shape are generally governed by the free energy that arises from the electrostatic or/and steric repulsion between the polyelectrolyte corona blocks and the excess free energy at the core–water interface.[18,21] Increasing the solvent ionic strength, or decreasing the length of the polyelectrolyte blocks, lowers the repulsive interactions between the polyelectrolyte chains of the corona, which increases the size of the micellar aggregate (Fig. 2c). Such an increase in the aggregate size implies the stretching of the core-forming chains in the radial direction[21] and leads to a conformational entropy loss in the core-forming blocks. The morphological transformation from spherical to cylindrical micelles, and further to lamella or vesicles, leads to further relaxation of the core blocks, which is energetically favored. The influence of the core-forming blocks on

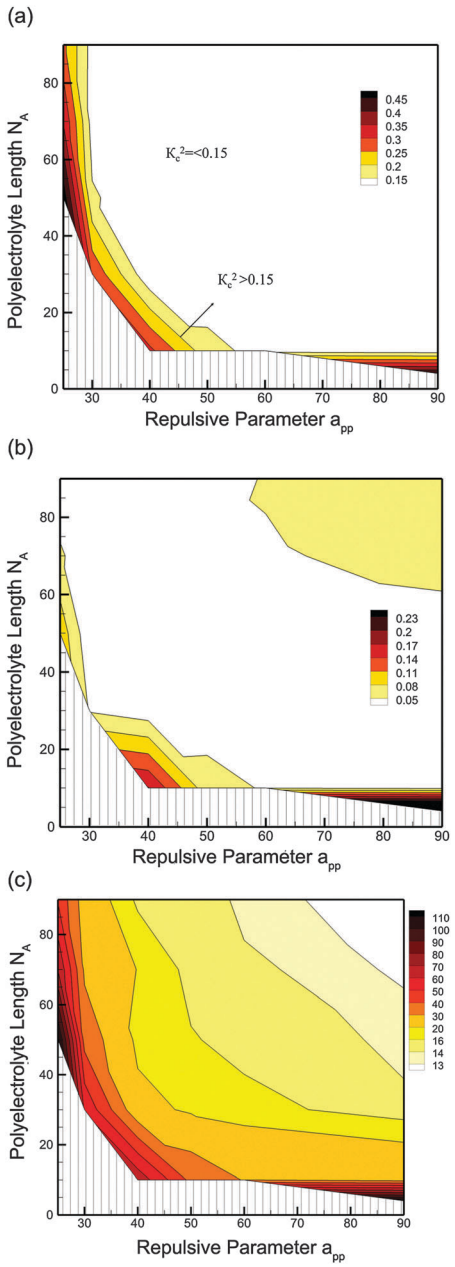

Fig. 2 Properties of micellar aggregates and morphological transitions represented as contour plots for anisotropy indices of (a) the micellar hydrophobic core, k_c^2 and (b) the whole micelle, k_m^2, and (c) the aggregation number, P. The region with aggregates formed by all chains in the system is shadowed.

the overall aggregate morphology becomes more pronounced when the size of the core exceeds that of the corona, or at high ionic strengths, as indicated at the bottom and the left side of the phase diagram. Our morphology phase diagram is consistent with the one proposed by Borisov and Zhulina's theory for PDCs with a very large hydrophobic block (N_B = 800) and variable polyelectrolyte blocks (N_A = 0–200) as a function of the effective second virial coefficient (excluded-volume parameter).[18,21] Our simulations show that even with a shorter hydrophobic block (N_B = 4), a similar morphological phase diagram can be obtained, which indicates that the morphological diagram presented in this paper may be generally valid.

The micellar morphology can be examined in terms of the anisotropy index κ^2, where κ^2 values range between 0 (completely spherical) and 1 (line) (see Experimental section). Fig. 2a shows the contour plot of the anisotropy index, ${\kappa_c}^2$, for the micellar hydrophobic cores. In our study we define spherical micelles as micelles with ${\kappa_c}^2 \leq 0.15$, whereas micelles with ${\kappa_c}^2 > 0.15$ are wormlike or cylindrical. Fig. 2a shows that as a_{pp} or N_A increases in the wormlike/cylindrical region, ${\kappa_c}^2$ becomes smaller, indicating that the core approaches a more spherical shape. However, the analysis of the change in the overall micellar anisotropy, ${\kappa_m}^2$, in Fig. 2b, indicates that the polyelectrolyte shell of the corona influences the shape of the micelles and that the ${\kappa_m}^2$ is quantitatively smaller than ${\kappa_c}^2$. In addition, an increase in ${\kappa_m}^2$, which occurs with long polyelectrolyte blocks at low ionic strengths (upper right hand corner of Fig. 2b), reflects the formation of star-like micelles, as shown in the upper-right region in the morphological phase diagram (Fig. 1e).

The equilibrium micellar aggregation number is determined by a free energy balance between the core and corona.[51] Fig. 2c shows a contour plot of the averaged aggregation number, P, as a function of polyelectrolyte repulsive parameter, a_{pp}, and polyelectrolyte length, N_A. We observed that the average aggregation number decreases with increasing strength of the repulsive interactions, a_{pp}, *i.e.*, decreasing solvent ionic strength. Changing the hydrophilic polyelectrolyte block length from 4 to 90, decreases the average aggregation number, which is also consistent with trends observed for neutral block copolymers.[52]

The average size of a micelle is determined by an interplay between an increase in the aggregation number and polyelectrolyte chain relaxation due to electrostatic screening. When the polyelectrolyte block is short ($N_A < 30$), the micellar radius of gyration, $R_{g,m}$, decreases as a_{pp} increases due to an increase in the aggregation number and the shape transitioning from cylindrical to spherical micelles (Fig. S5, ESI†). However, for a relatively long polyelectrolyte block ($N_A \geq 30$), an increase in the $R_{g,m}$ of spherical micelles is observed as a_{pp} increases due to the extension of micellar corona caused by electrostatic repulsion within and between polyelectrolyte chains.

Our model allows us to derive scaling functions between different micellar parameters for spherical micelles. The contour plot of the ratio of H_{corona}, defined as $H_{corona} = R_{g,m} - R_{g,c}$, to the core radius $R_{g,c}$ (Fig. S6, ESI†) indicates that the observed spherical aggregates represent an intermediate state between star-like ($H_{corona} \gg R_{g,c}$) and crew-cut ($H_{corona} \ll R_{g,c}$) micelles. For spherical micelles, scaling functions between micellar size parameters (H_{corona}, $R_{g,c}$, and $R_{g,m}$), the repulsive parameter a_{pp}, solvent ionic strength c_s, (where $a_{pp} = a_{ii} + a_{elec}$, and $a_{elec} \sim {c_s}^{-1}$), or the length of the polyelectrolyte block N_A can be used to predict the parameters of other micelles not pictured on the morphological diagram (Fig. 3). The derived scaling exponents associated with eqn (7)–(12) are listed in Tables 1 and 2.

For all spherical micelles, we determined the scaling relations between the corona thickness, and the solvent ionic strength and the length of polyelectrolyte block (Fig. 3a):

$$H_{corona} \sim {c_s}^{-0.11} {N_A}^{0.75} \quad (7)$$

$$H_{corona} \sim {a_{pp}}^{0.2} \quad (8)$$

Our results indicate that an increase in a_{pp} or N_A leads to an increase in the corona thickness (H_{corona}) despite the reduction in the aggregation number; hence, the length increase of the polyelectrolyte chains due to stretching, has a greater influence on corona thickness than the reduction of the aggregation number. Borisov and Zhulina[18] obtained a scaling relationship for the thickness of corona in the crew-cut limit, $H_{corona} \sim {N_A}^{0.8} \nu^{0.2}$, where $\nu = \nu_A + \frac{1}{2c_S}$ is the second virial coefficient for highly charged polyelectrolyte blocks. In our model, the repulsive parameter between charged DPD beads, a_{pp}, is the analog to ν in the Borisov and Zhulina model. Thus, our scaling exponents for a_{pp} or N_A and H_{corona} are in good agreement with the theory. Moreover, the observed scaling relation for $H_{corona} \sim {c_s}^{-0.11}$ is in general agreement with the experimental observations. For example, Förster *et al.*[53] reported that at salt concentrations above 0.05 M, *i.e.*, in the salt-dominated regime, $H_{corona} \sim {c_s}^{-0.13}$ for poly(ethylethylene-*b*-styrenesulfonic acid) (PEE–PSSH) micelles. Cristobal *et al.*[54] reported a weaker dependence on ionic strength ${c_s}^{-0.08}$ for poly(*n*-butyl acrylate)-*b*-poly(acrylic acid) (PBA3K-*b*-PAA12K) micelles with a weakly charged poly(acrylic acid) block.

We observed that for spherical PDC micelles, $R_{g,c}$ generally decreased with an increase of the repulsive parameter a_{pp} or N_A (Fig. S7, ESI†). The observed decrease of the micellar core size results from the combined effect of a decrease in the aggregation number and a compaction of the core. We note that when $a_{pp} \geq 50$, there is a slight increase in $R_{g,c}$ when N_A is increased from 70 to 90 (Fig. S7b, ESI†). This may be caused by a significant stretching of the longer polyelectrolyte chains which reduces the compactness of the core region. The lengths of short hydrophilic blocks, however, can have a strong influence on the core size $R_{g,c}$. Interestingly, the $R_{g,c}$ values are very close when $N_A \geq 30$ for the same solvent ionic strength. In the mean-field theory for neutral diblock copolymers, the $R_{g,c}$ is strongly dependent on the hydrophilic block length; whereas in scaling theory the $R_{g,c}$ is independent on the hydrophilic block length.[51] Our observations indicate a crossover between the mean-field theory and the scaling behavior of the micelles which is consistent with the previous studies for diblock copolymers.[24,55]

The effect of ionic strength on the radius of gyration of the micelles ($R_{g,m}$) is complex for the intermediate spherical micelles in this study (Fig. 3b). As discussed above, decreasing ionic

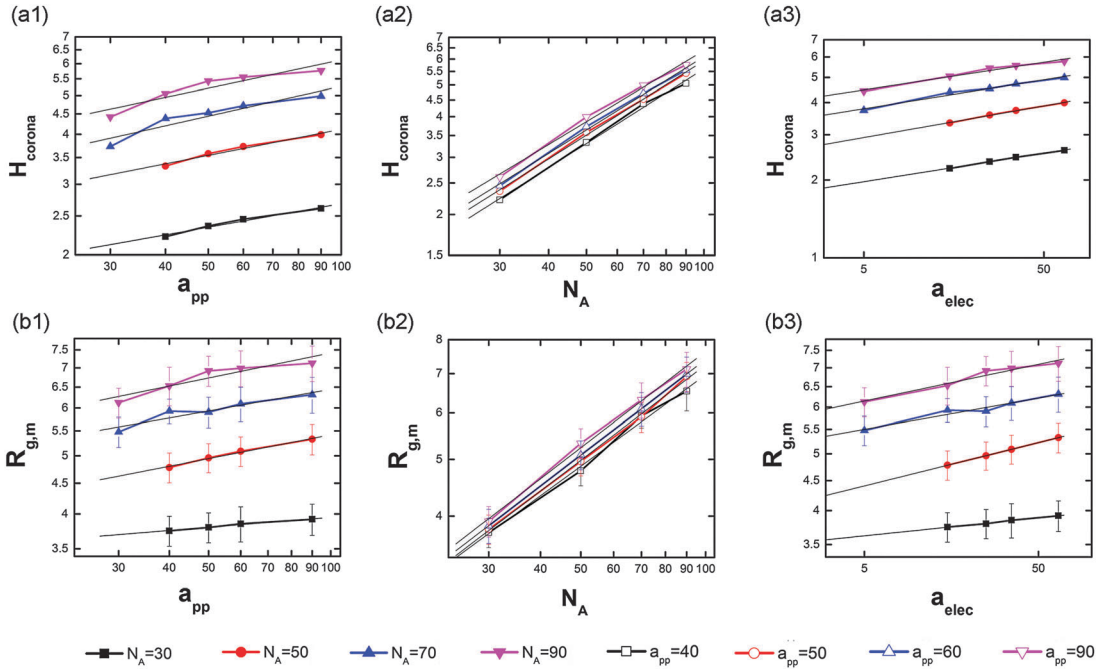

Fig. 3 The thickness of corona (H_{corona}) of spherical PDC micelles as a function of (a1) repulsive parameter a_{pp}, (a2) length of polyelectrolyte block N_A, and (a3) a_{elec}. The radius of gyration ($R_{g,m}$) of micelles as a function of a_{pp} (b1), N_A (b2), and a_{elec} (b3). Electrostatic repulsive parameter $a_{elec} \sim c_s^{-1}$.

Table 1 Dependence of the scaling exponents for H_{corona} and $R_{g,m}$ on the repulsive parameter a_{pp} and solvent ionic strength c_s. (Represented by the electrostatic repulsive parameter a_{elec}, $c_s \sim a_{elec}^{-1}$)

	Scaling exponential factor between	
Repulsive parameter, a_{pp}	H_{corona} and N_A	$R_{g,m}$ and N_A
40	0.761	0.518
50	0.758	0.540
60	0.746	0.542
90	0.725	0.545

Table 2 The dependence of the scaling exponents for $R_{g,m}$ and H_{corona} on the polyelectrolyte length N_A

	Scaling exponential factor between			
N_A	H_{corona} and a_{pp}	$R_{g,m}$ and a_{pp}	H_{corona} and c_s	$R_{g,m}$ and c_s
30	0.196	0.055	−0.111	−0.031
50	0.217	0.132	−0.123	−0.074
70	0.248	0.120	−0.112	−0.053
90	0.235	0.139	−0.107	−0.063

strength leads to a decrease in the core size and an increase in the thickness of the corona of micelles. The tradeoff between these two effects leads to the relationship between $R_{g,m}$ and solvent ionic strength. For star-like micelles, $R_{g,m}$ is expected to increase weakly with decreasing ionic strength (*i.e.*, increasing a_{pp}) due to the stretching of the chains in the corona, whereas for the crew-cut micelles, a decrease in core size also leads to a decrease in $R_{g,m}$, as the ionic strength decreases.[18] For $N_A = 30$ the system behaves more like crew-cut micelles and only a very weak increase in $R_{g,m}$ is observed as a_{pp} increases (Fig. 3b1). As the hydrophilic block length increases, the system starts to behave more like star-like micelles, so a stronger dependence of $R_{g,m}$ on a_{pp} or c_s was observed. Overall, the observed scaling relations between the size of spherical micelles and solvent ionic strength and the length of polyelectrolyte block are:

$$R_{g,m} \sim a_{pp}^{0.05}, \quad \text{for } N_A = 30 \tag{9}$$

$$R_{g,m} \sim a_{pp}^{0.13}, \quad \text{for } N_A > 30 \tag{10}$$

$$R_{g,m} \sim c_s^{-0.03} N_A^{0.54}, \quad \text{for } N_A = 30 \tag{11}$$

$$R_{g,m} \sim c_s^{-0.06} N_A^{0.54}, \quad \text{for } N_A > 30 \tag{12}$$

The theoretically predicted scaling relationship in Borisov and Zhulina's theory for star-like micelle is $R_{g,m} \sim N_A^{0.5455} \nu^{0.091}$.[18] While the observed $R_{g,m}$ *versus* length of polyelectrolyte block dependence has an excellent agreement with the theory, the exponent for a_{pp} (equivalent of ν) in our study is slightly larger than predicted for star-like micelles (Fig. 3b1). A weak dependence of the micelle radius ($R_{g,m}$) on solvent ionic strength is noticeable at intermediate micellar morphologies, *i.e.*, when $H_{corona}/R_{g,c}$ ranges from 0.50 to 4.22 for spherical micelles. The weak dependence of R_h on ionic strength was also observed in previous experimental studies of PIB30-*b*-PMAA170 micelles, *i.e.*, $R_h \sim c_s^{-0.07}$.[12] Also, our H_{corona} and $R_{g,m}$ scaling relations are similar to those reported by Colombani *et al.*[56] for the self-assembly of diblock copolymers poly(*n*-butyl acrylate)-*block*-poly(acrylic acid) (PnBA-PAA): $H_{corona} \sim DP_{PAA}^{0.7}$, $R_{g,m} \sim DP_{PAA}^{0.6}$, $R_h \sim DP_{PAA}^{0.5}$, where $DP_{PAA} = N_A$ is the length of the polyelectrolyte block. Therefore, the exponent of the power law behavior of micelle radius ($R_{g,m}$) on solvent ionic strength depends on the length of the ionic block for spherical micelles at an

intermediate state between star-like ($H_{corona} \gg R_{g,c}$) and crew-cut ($H_{corona} \ll R_{g,c}$) micelles.

To validate the predicted phase diagram, we compare the micellar morphology formed by highly asymmetric, 54-mer diblock polyelectrolytes using simulations and experiments. For this diblock length ($N_A = 50$ and $N_B = 4$), our simulations indicate a change in micellar morphology with increasing a_{pp} (*i.e.*, decreasing solvent ionic strength) (Fig. 1e). At high ionic strength the PDCs form large micelles with aspherical cores, whereas at lower solvent ionic strength, the PDCs form spherical micelles. To verify the predicted changes we used $(F\text{-dUTP})_4$-*b*-$polyT_{50}$, a polynucleotide block copolymer, which has a hydrophilic, 50-mer polynucleotide block ($polyT_{50}$), appended with a short, hydrophobic oligonucleotide block (F-dUTP), which contains about 4 hydrophobic unnatural nucleotides. A combination of AFM and SLS was employed to observe the changes in micelle morphology of $(F\text{-dUTP})_4$-*b*-$polyT_{50}$ as a function of monovalent salt concentration (*i.e.* NaCl) for a range of charge ratios, λ, defined as the ratio of charges along the polynucleotide backbones, c_p^m, to the monovalent salt concentration, c_s^m (Fig. 4). The charge ratio λ, represents the ionic strength, and is an experimental analog of the a_{elec} in the DPD simulations. In Fig. 4a, we plot the $R_{g,m}$ obtained from SLS as a function of charge ratio λ, and $R_{g,m}$ obtained from the simulation as a function of a_{pp}. In addition to SLS, the assemblies were also visualized by AFM tapping mode height imaging in air at three different charge ratios λ (Fig. 4b–d).[24] We also determined the average diameters and heights of the aggregates and micelles from AFM images (Table S1, ESI†).

Depending on the solvent ionic strength, our results reveal two distinct regimes for self-assembly of 54-mer PDCs. The first regime occurs at high solvent ionic strength ($\lambda = 6.1 \times 10^{-5}$ and $a_{pp} \leq 30$), where the repulsion between the polyelectrolyte chains and between adjacent micelles is reduced due to screening effects, which allows for the formation of large, micellar aggregates (Fig. 4b). Similar micellar aggregation behavior has been observed by cryo-transmission electron microscopy (cryo-TEM) for ethylethylene-*b*-styrenesulfonic acid (PEE-PSSH) at a high salt concentration.[53] The second regime occurs at lower salt concentration ($\lambda \geq 3.1 \times 10^{-3}$ and $a_{pp} > 30$), where there still is significant Coulomb repulsion between charged polyelectrolyte chains, and the micelle formation is driven by the interplay between electrostatic repulsion of charged blocks, and association of hydrophobic blocks, which results in homogeneously distributed, individual spherical micelles (Fig. 4c and d).

To determine the effect of ionic strength on the size of the self-assembled PDC micelles in aqueous solution we compare the salt-dependent changes in the radius of gyration ($R_{g,m}$) of micelles obtained from SLS and DPD simulations. At low ionic strengths (*i.e.*, $\lambda > 1 \times 10^{-3}$ and $a_{pp} > 30$), the $R_{g,m}$ moderately decreases with increasing salt concentration due to the increased screening of electrostatic interactions between the negatively charged polyelectrolytes. This decrease in $R_{g,m}$ reflects the gradual collapse of the micellar corona with increasing ionic strength. Upon further increase in salt concentration, the $R_{g,m}$ increases sharply, which reflects micellar aggregation and perhaps a morphological transition, induced by the decrease in electrostatic repulsion (vertical dash line in Fig. 4a). Overall, the qualitative agreement for salt-dependent changes in the size of micelles between experiment and simulations is analogous, further validating our simulation approach.

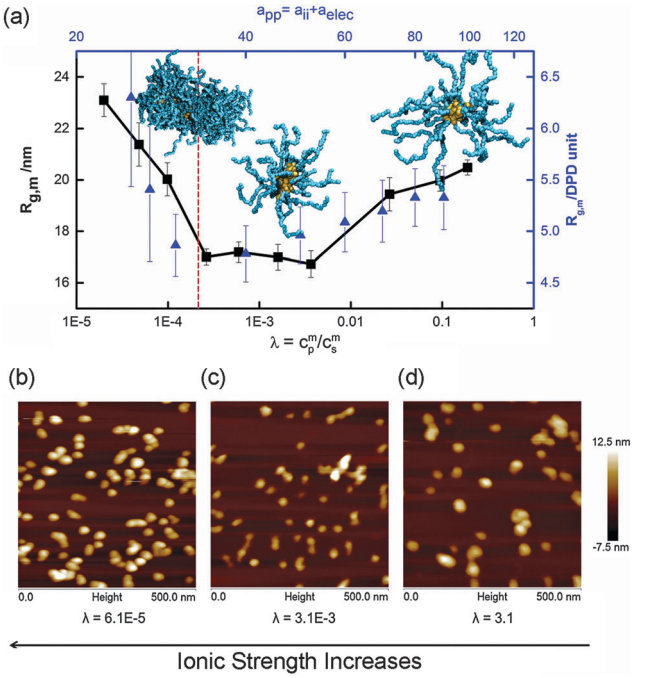

Fig. 4 (a) Radius of gyration for F-dUTP-*b*-polyT50 micelles determined from SLS (black squares) and from DPD simulations (blue triangles) plotted as a function of the charge ratio λ (bottom) and repulsive parameter a_{pp} (top). The vertical dashed line indicates the predicted change in micellar morphology. (b–d) AFM tapping mode height images of spherical micelles and aggregates at three different charge ratios.

Conclusions

Here the prediction of the salt-responsive morphologies of aggregates or micelles formed by amphiphilic diblock copolymers was achieved using ISIS DPD methodology. The copolymers in this study comprise of a short hydrophobic block and a polyelectrolyte hydrophilic block of varying lengths from 4-mer to 90-mer in aqueous solutions. We found that the morphology of the self-assembled structures undergoes transitions from spherical micelles to cylindrical micelles to lamellar aggregates with increasing solvent ionic strength or decreasing polyelectrolyte block length. Spherically shaped micelles were obtained over a wide area in the diagram due to the short length of the hydrophobic part. Quantitative evaluation of the micelle radius of gyration, $R_{g,m}$ and corona thickness, H_{corona}, and their scaling law dependence on the solvent ionic strength c_s or the length of the polyelectrolyte block N_A were obtained. For all spherical micelles a scaling relation $H_{corona} \sim c_s^{-0.11} N_A^{0.75}$ was obtained. The length of polyelectrolytes played a role in a scaling relationship between radius of gyration and a solvent ionic strength, where for $N_A = 30$, a scaling relation of $R_{g,m} \sim c_s^{-0.03} N_A^{0.54}$ was observed, while for $N_A > 30$, $R_{g,m} \sim c_s^{-0.06} N_A^{0.54}$.

To verify the model predictions, we studied the self-assembly behavior of polyT50-*b*-F-dUTP in aqueous solution as a function of solvent ionic strength. The micellar dimensions, determined from AFM and SLS measurements, showed the same conformational transitions and dependence on ionic strength as the computational prediction for a 54-mer PDC. This excellent qualitative agreement between experiment and simulations further validates our ISIS DPD simulations, and suggests that the ISIS DPD method can be used as a powerful tool to guide the rational design of solvent-responsive polyelectrolyte block copolymer nanostructures.

Abbreviations

PDC Polyelectrolyte diblock copolymer
DPD Dissipative particle dynamics

Acknowledgements

This work was supported by the NSF DMR-1410462, NSF's Research Triangle MRSEC (DMR-1121107) and NSF CMMI-1150682. The computer support was provided by the High Performance Computing Center at North Carolina State University. The authors thank Isaac Weitzhandler for his help with SLS measurements.

References

1 P. Alexandridis and B. Lindman, *Amphiphilic Block Copolymers*, Elsevier Science B.V., Amsterdam, 2000.
2 K. Hales and D. J. Pochan, *Curr. Opin. Colloid Interface Sci.*, 2006, **11**, 330–336.
3 M. A. C. Stuart, B. Hofs, I. K. Voets and A. de Keizer, *Curr. Opin. Colloid Interface Sci.*, 2005, **10**, 30–36.
4 S. M. Loverde, D. A. Pantano, D. A. Christian, A. Mahmud, M. L. Klein and D. E. Discher, *Curr. Opin. Solid State Mater. Sci.*, 2011, **15**, 277–284.
5 Y. Geng, P. Dalhaimer, S. S. Cai, R. Tsai, M. Tewari, T. Minko and D. E. Discher, *Nat. Nanotechnol.*, 2007, **2**, 249–255.
6 S. Y. Yu-Su, D. R. Thomas, J. E. Alford, I. Larue, M. Pitsikalis, N. Hadjichristidis, J. M. DeSimone, A. V. Dobrynin and S. S. Sheiko, *Langmuir*, 2008, **24**, 12671–12679.
7 T. Lohmuller, D. Aydin, M. Schwieder, C. Morhard, I. Louban, C. Pacholski and J. P. Spatz, *Biointerphases*, 2011, **6**, Mr1–Mr12.
8 S. Mura, J. Nicolas and P. Couvreur, *Nat. Mater.*, 2013, **12**, 991–1003.
9 Y. Z. Zhu, D. Wang, L. Jiang and J. Jin, *NPG Asia Mater.*, 2014, **6**, e101.
10 K. Khougaz, I. Astafieva and A. Eisenberg, *Macromolecules*, 1995, **28**, 7135–7147.
11 L. Zhang and A. Eisenberg, *Science*, 1995, **268**, 1728–1731.
12 M. Burkhardt, N. Martinez-Castro, S. Tea, M. Drechsler, I. Babin, I. Grishagin, R. Schweins, D. V. Pergushov, M. Gradzielski, A. B. Zezin and A. H. E. Müller, *Langmuir*, 2007, **23**, 12864–12874.
13 V. Schmidt, E. Di Cola, C. Giacomelli, A. R. Brisson, T. Narayanan and R. Borsali, *Macromolecules*, 2008, **41**, 2195–2202.
14 T. Bonné, K. Lüdtke, R. Jordan, P. Štěpánek and C. Papadakis, *Colloid Polym. Sci.*, 2004, **282**, 1425.
15 J. H. Jeong and T. G. Park, *Bioconjugate Chem.*, 2001, **12**, 917–923.
16 S. Pispas and N. Hadjichristidis, *Macromolecules*, 2003, **36**, 8732–8737.
17 I. Hamley, *Block Copolymers in Solution: Fundamentals and Applications*, John Wiley & Sons, Ltd, 2005, ch. 4, pp. 173–213, DOI: 10.1002/9780470016985.
18 O. Borisov, E. Zhulina, F. M. Leermakers and A. E. Müller, in *Self Organized Nanostructures of Amphiphilic Block Copolymers I*, ed. A. H. E. Müller and O. Borisov, Springer Berlin Heidelberg, 2011, vol. 241, ch. 114, pp. 57–129.
19 N. P. Shusharina, I. A. Nyrkova and A. R. Khokhlov, *Macromolecules*, 1996, **29**, 3167–3174.
20 N. P. Shusharina, P. Linse and A. R. Khokhlov, *Macromolecules*, 2000, **33**, 3892–3901.
21 O. V. Borisov and E. B. Zhulina, *Macromolecules*, 2003, **36**, 10029–10036.
22 O. V. Borisov and E. B. Zhulina, *Macromolecules*, 2002, **35**, 4472–4480.
23 E. B. Zhulina and O. V. Borisov, *Macromolecules*, 2012, **45**, 4429–4440.
24 L. Tang, V. Tjong, N. Li, Y. G. Yingling, A. Chilkoti and S. Zauscher, *Adv. Mater.*, 2014, **26**, 3050–3054.
25 C. Pons-Siepermann and S. C. Glotzer, *ACS Nano*, 2012, **6**, 3919–3924.
26 M. Dutt, O. Kuksenok, M. J. Nayhouse, S. R. Little and A. C. Balazs, *ACS Nano*, 2011, **5**, 4769–4782.
27 M. Tagliazucchi, M. O. de la Cruz and I. Szleifer, *Proc. Natl. Acad. Sci. U. S. A.*, 2010, **107**, 5300–5305.
28 A. Singh, S. Snyder, L. Lee, A. P. R. Johnston, F. Caruso and Y. G. Yingling, *Langmuir*, 2010, **26**, 17339–17347.
29 N. K. Li, H. S. Kim, J. A. Nash, M. Lim and Y. G. Yingling, *Mol. Simul.*, 2014, **40**, 777–783.
30 J. P. K. Doye, T. E. Ouldridge, A. A. Louis, F. Romano, P. Sulc, C. Matek, B. E. K. Snodin, L. Rovigatti, J. S. Schreck, R. M. Harrison and W. P. J. Smith, *Phys. Chem. Chem. Phys.*, 2013, **15**, 20395–20414.
31 D. A. Potoyan, A. Savelyev and G. A. Papoian, *WIREs Comput. Mol. Sci.*, 2013, **3**, 69–83.
32 G. A. Cisneros, V. Babin and C. Sagui, in *Biomolecular Simulations*, ed. L. Monticelli and E. Salonen, Humana Press, 2013, vol. 924, ch. 10, pp. 243–270.
33 R. D. Groot, *J. Chem. Phys.*, 2003, **118**, 11265–11277.
34 C. Ibergay, P. Malfreyt and D. J. Tildesley, *J. Phys. Chem. B*, 2010, **114**, 7274–7285.
35 L. T. Yan and X. J. Zhang, *Soft Matter*, 2009, **5**, 2101–2108.
36 P.-Y. Hsiao, *Macromolecules*, 2006, **39**, 7125–7137.
37 X. Jiang, W. Qu, D. Pan, Y. Ren, J. M. Williford, H. G. Cui, E. Luijten and H. Q. Mao, *Adv. Mater.*, 2013, **25**, 227–232.

38 D. A. Pantano, M. L. Klein, D. E. Discher and P. B. Moore, *J. Phys. Chem. B*, 2011, **115**, 4689–4695.
39 N. K. Li, W. H. Fuss and Y. G. Yingling, *Macromol. Theory Simul.*, 2015, **24**, 7–12.
40 http://lammps.sandia.gov.
41 S. Plimpton, *J. Comput. Phys.*, 1995, **117**, 1–19.
42 P. J. Hoogerbrugge and J. M. V. A. Koelman, *Europhys. Lett.*, 1992, **19**, 155–160.
43 R. D. Groot and P. B. Warren, *J. Chem. Phys.*, 1997, **107**, 4423–4435.
44 P. B. Warren, *Phys. Rev. E: Stat., Nonlinear, Soft Matter Phys.*, 2003, **68**, 066702.
45 G. Kacar, E. A. J. F. Peters and G. de With, *EPL*, 2013, **102**, 40009.
46 N. Li, C. Zuo and Q. Cao, *J. Macromol. Sci., Phys.*, 2012, **51**, 275–287.
47 Q. Cao, C. Zuo, L. Li, Y. Yang and N. Li, *Microfluid. Nanofluid.*, 2011, **10**, 977–990.
48 C. M. Wijmans, B. Smit and R. D. Groot, *J. Chem. Phys.*, 2001, **114**, 7644–7654.
49 M. González-Melchor, E. Mayoral, M. E. Velazquez and J. Alejandre, *J. Chem. Phys.*, 2006, **125**, 224107.
50 P. P. Ewald, *Ann. Phys.*, 1921, **64**, 253–287.
51 G. Riess, *Prog. Polym. Sci.*, 2003, **28**, 1107–1170.
52 C. Booth and D. Attwood, *Macromol. Rapid Commun.*, 2000, **21**, 501–527.
53 S. Förster, N. Hermsdorf, C. Bottcher and P. Lindner, *Macromolecules*, 2002, **35**, 4096–4105.
54 G. Cristobal, J.-F. Berret, C. Chevallier, R. Talingting-Pabalan, M. Joanicot and I. Grillo, *Macromolecules*, 2008, **41**, 1872–1880.
55 L. Willner, A. Poppe, J. Allgaieri, M. Monkenbusch, P. Lindner and D. Richter, *Europhys. Lett.*, 2000, **51**, 628–634.
56 O. Colombani, M. Ruppel, M. Burkhardt, M. Drechsler, M. Schumacher, M. Gradzielski, R. Schweins and A. H. E. Müller, *Macromolecules*, 2007, **40**, 4351–4362.

